nature microbiology

Article

https://doi.org/10.1038/s41564-022-01317-3

L-form conversion in Gram-positive bacteria enables escape from phage infection

Received: 12 May 2022

Accepted: 22 December 2022

Published online: 30 January 2023

Check for updates

Jan C. Wohlfarth[1], Miki Feldmüller[2], Alissa Schneller[1], Samuel Kilcher[1], Marco Burkolter[1], Susanne Meile[1], Martin Pilhofer[2], Markus Schuppler[1] & Martin J. Loessner[1]

At the end of a lytic bacteriophage replication cycle in Gram-positive bacteria, peptidoglycan-degrading endolysins that cause explosive cell lysis of the host can also attack non-infected bystander cells. Here we show that in osmotically stabilized environments, *Listeria monocytogenes* can evade phage predation by transient conversion to a cell wall-deficient L-form state. This L-form escape is triggered by endolysins disintegrating the cell wall from without, leading to turgor-driven extrusion of wall-deficient, yet viable L-form cells. Remarkably, in the absence of phage predation, we show that L-forms can quickly revert to the walled state. These findings suggest that L-form conversion represents a population-level persistence mechanism to evade complete eradication by phage attack. Importantly, we also demonstrate phage-mediated L-form switching of the urinary tract pathogen *Enterococcus faecalis* in human urine, which underscores that this escape route may be widespread and has important implications for phage- and endolysin-based therapeutic interventions.

In natural environments, bacteria are challenged by bacteriophages, which exert strong selective pressure on microbial communities. Indeed, phage-induced lysis is thought to be the most frequent cytocidal event in the biosphere[1]. The biology of phage infection has been subject to extensive studies and begins with phage attachment to the bacterial host surface by binding to a suitable receptor. In Gram-positive bacteria, host surface recognition typically involves carbohydrates that are covalently linked to the peptidoglycan cell wall, such as teichoic acids[2–4]. Receptor binding is essential and without it, infection cannot be initiated. After attachment, the phage genome is injected into the host followed by expression of viral genes and assembly of new virions. To be released to the environment, progeny phages have to escape from their bacterial host cell. However, the cell wall and cytoplasmic membrane represent natural barriers preventing dissemination. Therefore, the tailed bacteriophages (*Caudovirales*) have evolved a canonical set of lysis proteins, designated as the holin-endolysin system, which typically mediates host cell destruction by cell wall hydrolysis[5,6]. Endolysins are peptidoglycan hydrolases that specifically recognize and cleave the bacterial cell wall. The structure of these proteins is highly modular and typically consists of an N-terminal enzymatically active domain (EAD) and a C-terminal cell wall binding domain (CBD) which promotes substrate specificity[7–9]. Access of endolysins to their substrate must be tightly regulated and depends on the assembly of holins in the cytoplasmic membrane at the end of the lytic cycle. This leads to pore formation, membrane depolarization and access of endolysin to the cell wall, facilitating immediate degradation of the peptidoglycan[5,7,10]. Together, these effects result in explosive cell lysis of the host[8,11,12].

Remarkably, recent studies have demonstrated that phage-induced lysis may concomitantly also result in a massive release of bacterial membrane vesicles (MV) from both Gram-positive and Gram-negative bacterial cells[12,13]. These MVs incorporate cytosolic content including genomic DNA, thus sharing some similarity with cell wall-deficient L-form cells[11]. However, the potential role of L-form switching in the natural interaction of bacteria with their phage predators has not been established. The available evidence shows that many bacteria may transiently enter a wall-deficient state in the presence of certain triggers, such as lytic enzymes or cell wall-active antibiotics[14,15]. Due to the lack of a cell wall and associated molecules, L-forms are

[1]Institute of Food, Nutrition and Health, ETH Zurich, Zurich, Switzerland. [2]Institute of Molecular Biology and Biophysics, ETH Zurich, Zurich, Switzerland. e-mail: martin.loessner@ethz.ch

intrinsically resistant to such peptidoglycan-targeting compounds. Therefore, L-form research has mostly addressed their possible role as persisters in chronic or recurrent infections[16–19]. While it has been pointed out previously that L-forms or wall-deficient cells may also confer resistance to phage infection[20–23], the biological relevance of this phenomenon remained elusive because no clear link between phage infection and L-form emergence has yet been demonstrated. Here we investigate the effects of phage infection on the emergence of bacterial L-forms, using *Listeria monocytogenes* and phage A006. We have recently developed a model for studying the biology of transient *L. monocytogenes* L-forms. These cells undergo an efficient L-form switch in the presence of an inducer, such as penicillin or lysozyme, while retaining the ability to revert to the walled state in the absence of selective pressure[24,25]. Remarkably, L-form proliferation neither requires a cell wall nor the dedicated FtsZ-driven cell division machinery[26]. Instead, proliferation seems to rely solely on continuous membrane synthesis and biophysical effects, where an increased surface area-to-volume ratio results in membrane protrusion and formation of internal or external vesicles as viable progeny[27,28]. Temperate *Listeria* phage A006 is a member of the *Siphoviridae*, featuring a 38.1 kb double-stranded DNA genome[29]. A recently developed L-form-based genomic rebooting platform allows facile and rapid genomic editing of this phage. Due to its genetic tractability, it has emerged as a model to study *L. monocytogenes* phage–host interactions[24,30,31].

Our results show that phage infection and cell lysis can trigger L-form conversion in bacterial populations, which confers resistance to further infection, and demonstrate that L-form conversion is also possible based on the activity of endolysin released during repeated cycles of phage infection. Mechanistically, liberated phage endolysins induce lesions in the cell walls of noninfected bystander cells, thereby promoting turgor-driven extrusion of wall-deficient cells. Importantly, phage-induced L-forms retain the ability to revert to the walled state in the absence of selective pressure. These effects are not restricted to *L. monocytogenes* but could also be observed in *Enterococcus faecalis* phage–host pairs. Together, our results suggest that Gram-positive bacteria can evade phage predation at the population level via transient switching of subpopulations to the L-form state.

Results

Wall-deficient cells released after bacteriophage infection

We initiated the current study by exploring the effect of virulent phage infection on the emergence of bacterial L-forms. These experiments were inspired by earlier observations that prophage-triggered cell lysis results in the emergence of bacterial membrane vesicles[13]. In principle, these vesicles comprise the minimum characteristics of cellular life including genomic DNA, cytosolic content and a cellular membrane[11], thereby resembling L-forms. However, previous work was performed in hypotonic environments, thus preventing the emergence of L-form cells due to osmotic cell lysis[12,13]. We therefore aimed to induce phage-induced L-form switching under osmoprotective conditions. We used *L. monocytogenes* strain EGD-e Rev2, which can undergo efficient L-form switching and reversion under variable selective conditions[24]. To ensure a strictly lytic bacteriophage phenotype, we used A006 ΔLCR, an engineered virulent derivative of temperate phage A006 that lacks its entire lysogeny control region[30]. To test our hypothesis, we developed a protocol in which we challenged Rev2 cells expressing chromosomally integrated eGFP (enhanced green fluorescent protein) with A006 ΔLCR in DM3 L-form medium containing succinate as an osmoprotectant and $CaCl_2$ to support phage infection[32–34]. Under such conditions, phage-induced lysis still resulted in degradation of the thick peptidoglycan layer while leaving the cytoplasmic membrane structurally intact (Fig. 1 and Supplementary Video 1). This led to the formation of wall-deficient cells that remained stable even after prolonged incubation periods (Fig. 1a and Supplementary Video 1). In contrast, phage infection in standard hypotonic medium (0.5 BHI) dramatically decreased the half-life of wall-deficient cells and resulted in rapid osmotic lysis (Fig. 1c). As expected, exposure to the parental temperate phage A006 yielded similar results, thus demonstrating that emergence of wall-deficient cells also occurs after infection with wild-type temperate phage during its lytic reproduction cycle (Fig. 1b).

Phage infection triggers L-form switching and proliferation

Following the above observations, we asked whether the wall-deficient vesicles observed in Fig. 1 in fact represented viable L-forms. A hallmark for L-form cells and a distinction from protoplasts is their ability to proliferate in the absence of a cell wall[35]. Therefore, we aimed to observe proliferation using time-lapse microscopy. Towards this end, Rev2 cells expressing eGFP were infected with phage A006 ΔLCR and incubated for 18 h to minimize the number of potential walled survivors that would overgrow the slow-growing L-forms. The culture was then transferred on osmoprotective agar for time-lapse microscopy, which demonstrated abundant wall-deficient cells undergoing shape deformations and irregular cell divisions characteristic for L-form growth[28] (Supplementary Fig. 1 and Supplementary Video 2). To confirm and quantify the observed effect for wild-type phage A006 (Fig. 4g), we infected Rev2 cells with serial dilutions of phage at $t = 0$ min and monitored the infection dynamics by time-course turbidity assays and plating of lysed cultures on DM3 agar at various timepoints (Fig. 2a,b). Curiously, we found that the fraction of L-form survivors increased with decreasing phage concentration (Fig. 2b). At high phage concentrations, when most bacteria should be infected during the first cycle, bacterial survivors were predominantly walled. In contrast, infections at lower phage concentrations predominantly resulted in L-form colonies, which were phenotypically discernible by their characteristic 'fried-egg' colony morphology (Fig. 2c,d). To explore whether these observations also hold true for other phages and bacterial species, we challenged *L. monocytogenes* Rev2 with several different phages including P35, P40, A118 (*Siphoviridae*) and A511 (*Myoviridae*). Moreover, to provide proof of principle for other Gram-positive bacteria, we challenged *Enterococcus faecalis*, which has also been reported to convert to L-forms[36], with the virulent *Enterococcus* phage Efs7 (*Siphoviridae*) (Fig. 4h). Again, we observed emergence of L-form colonies for all tested combinations of phages and host strains (Fig. 2f,g). Importantly, both *L. monocytogenes* and *E. faecalis* L-forms retained the ability to switch back to the walled state, indicating that removal of selective pressure allows for reversion to the walled phenotype (Fig. 2e–h).

L-form escape is mediated by endolysin damage

Our observation of phage-induced L-form conversion raised the question regarding its primary effector. Phage-encoded endolysins are highly active peptidoglycan hydrolases and have been shown to trigger the release of bacterial membrane vesicles[12,13]. Therefore, we speculated that the concomitant release and temporal accumulation of endolysins following repeated infection cycles may be involved in the formation of L-forms in a similar manner. This idea was supported by our observation that infections at low initial phage concentrations increase the fraction of L-form survivors compared with higher concentrations of applied phage (Fig. 2c). To investigate the effect of endolysins on L-form emergence, we produced recombinant phage A006-derived endolysin Ply006[37] and Efs7-derived endolysin Ply007 (both C-terminally fused to a 6xHis-tag) (Fig. 3f). Next, we challenged intact *L. monocytogenes* Rev2 and *E. faecalis* cells with serial dilutions of the respective purified endolysin (Fig. 3a,b). On the basis of the linear ranges of the enzymes in $DM3_{\Phi}$, we determined a specific activity of approximately 0.4 $\Delta OD_{600}\ min^{-1}\ \mu M^{-1}$ for both Ply006 and Ply007 (Fig. 3c), demonstrating the high activity of the enzymes on their specific cell wall substrate. To test whether endolysin-mediated lysis promotes L-form generation, we then plated lysed bacterial cultures on osmoprotective DM3 agar. Indeed, L-form colonies could be observed at high frequency (approximately 1–2% of lysed cells) after 2–5 d

https://doi.org/10.1038/s41564-022-01317-3

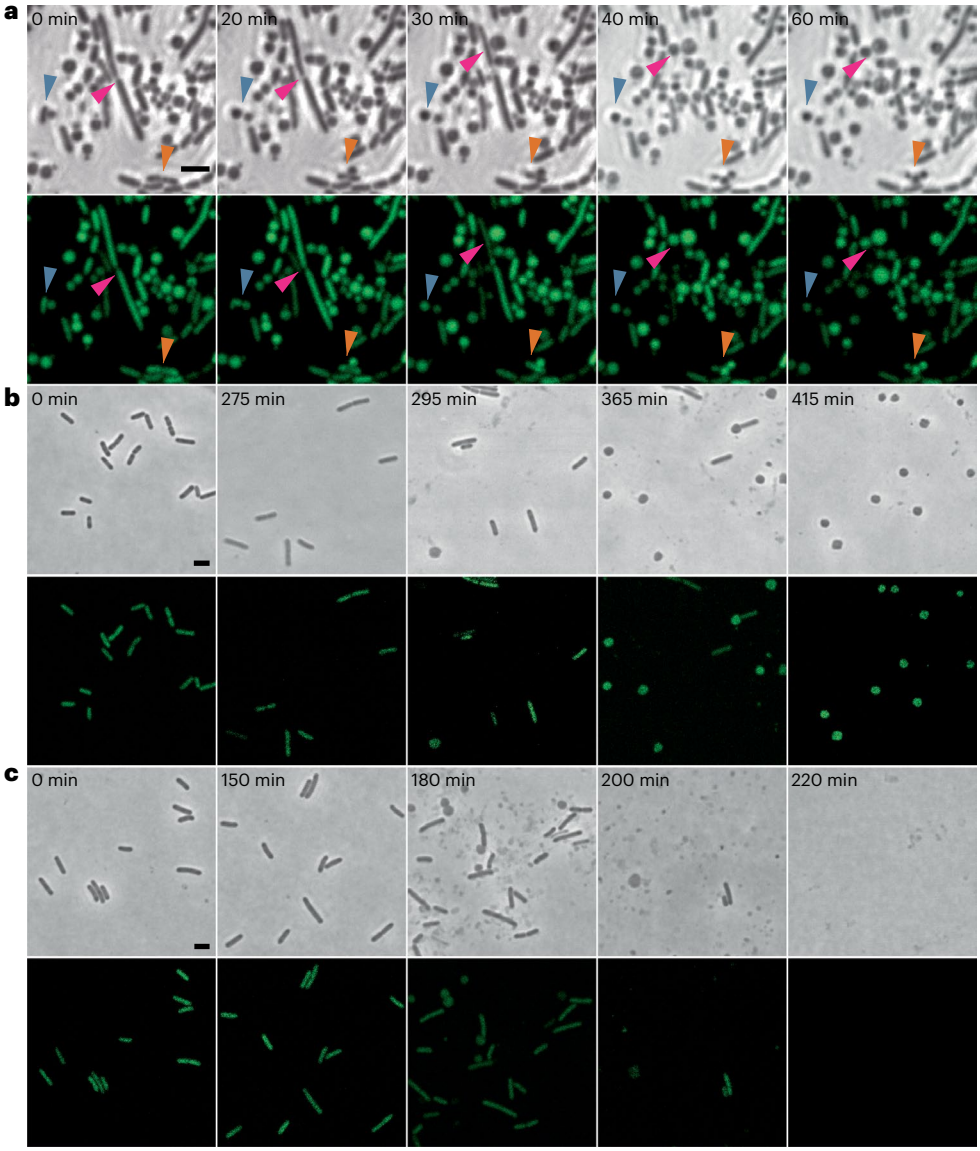

Fig. 1 | Phage-induced lysis leads to formation of wall-deficient bacterial cells under osmoprotective conditions. a, The effects of infection with a lytic phage on the transition of *L. monocytogenes* Rev2 to wall-deficient bacterial cells under osmoprotective conditions. Cells expressing chromosomally integrated eGFP were challenged with a strictly lytic mutant of temperate *Listeria* phage A006 lacking the lysogeny control region (ΔLCR) in osmoprotective $DM3_{\Phi}$ medium. Turbidity was monitored by spectrophotometry and before lysis, and cells were placed on DM3 agar for time-lapse microscopy ($t = 0$ min). Shown are phase contrast (PC) micrographs (top) and the corresponding channel for green light emission (bottom). Individual bacterial transition events are denoted by red, orange and blue arrows. Individual frames were extracted from Supplementary Video 1. **b**,**c**, Contrary effects of hypotonic vs osmoprotective medium on phage-induced wall-deficient cells. *L. monocytogenes* Rev2 cells expressing chromosomally integrated eGFP were infected with temperate phage A006 in osmoprotective $DM3_{\Phi}$ medium (**b**) or standard hypotonic 0.5 BHI medium (**c**). Cells were sampled at several timepoints before and after phage-induced bacterial lysis, followed by microscopic examination on 0.5 BHI or DM3 agar pads, respectively. In hypotonic medium, transition to the wall-deficient state is accompanied by rapid lysis, whereas under osmoprotective conditions, transition to the wall-deficient state is observed and most cells remain intact. Shown are PC images (top) and the corresponding channel for green light emission (bottom). The figures are representative of at least three independent experiments. Scale bars, 2 µm.

incubation for both *E. faecalis* and Rev2 (Fig. 3d,e). Endolysin-induced L-forms generally retained the ability to revert to the walled state, which presumably reflects the gradual loss of enzymatic activity (Supplementary Fig. 2e,f). These results demonstrated that endolysins can act as efficient 'transforming agents' for L-form conversion.

Endolysin-induced cell wall lesions enable L-form generation

To get a mechanistic insight into endolysin-mediated L-form switching, we exposed walled *L. monocytogenes* Rev2 cells expressing eGFP or *E. faecalis* cells to 1 µM Ply006 or Ply007, respectively, and followed L-form escape via single-cell resolution time-lapse microscopy. We observed that under osmoprotective conditions, endolysin-mediated L-form conversion typically started with a blebbing process, resulting in extrusion of the cytoplasmic membrane from the cell wall sacculus, followed by proliferation of the wall-deficient cells. In addition, we occasionally observed transition events following explosive cell lysis (Fig. 3h,j,k and Supplementary Videos 4a,b, 6 and 7). In contrast, endolysin treatment under hypotonic conditions usually led to sudden osmotic rupture, disintegration of membrane vesicles and cell death. This corroborates the initial finding that stability of phage-induced L-forms is dependent on osmoprotective environments (Fig. 3g,i and Supplementary Videos 3 and 5). To investigate the ultrastructural

https://doi.org/10.1038/s41564-022-01317-3

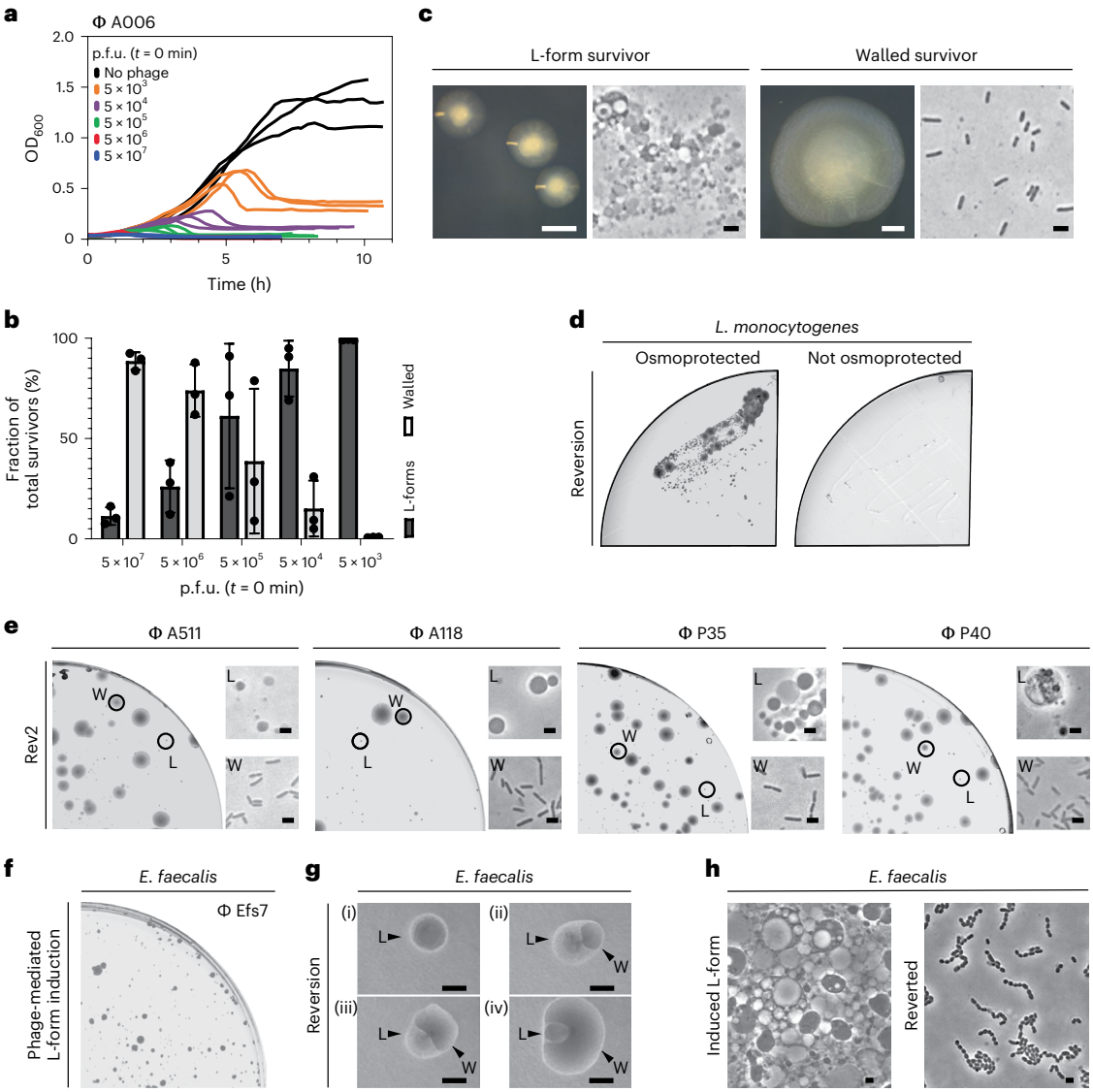

Fig. 2 | Phage infection triggers bacterial L-form switching. a–**c**, L-form switching of *L. monocytogenes* Rev2 in response to phage A006 infection. **a**, Growth curves in liquid culture. Bacteria were challenged with 10-fold serial dilutions of phage (p.f.u.) or no phage at $t = 0$ min. For each dilution, three independent replicates are presented as individual curves. **b**, Relative quantification of bacterial colony forming units (c.f.u.) on DM3 agar. L-forms and walled survivors are normalized to the number of total c.f.u. per infection. Values are displayed as mean ± s.d. of three biological replicates. Each culture was plated on osmoprotective DM3 agar 5 h after reaching maximum OD_{600}. Walled colonies were enumerated after 2 d, L-forms after 5 d. **c**, Micrographs depict colony phenotypes (left) and cell morphology (right) of L-forms and walled cells as observed in **b**. **d**, Phage-induced *L. monocytogenes* Rev2 L-forms retain the ability to revert to the walled state in the absence of selective pressure. Shown is a restreak of a single survivor L-form colony obtained from **b** on osmoprotective DM3 agar and hypotonic 0.5 BHI agar. Note that numerous reverted walled colonies as well as non-reverted L-form colonies emerge on DM3 agar plates after 5 d. In contrast, no colonies emerge on 0.5x BHI agar, ruling out the possible presence of remnant walled cells in the analysed colonies. **e**, Infection of *L. monocytogenes* Rev2 with phage A511, A118, P35 or P40 triggers L-form switching. Plates were imaged at 5 d post infection and are representative of individual infections at 5×10^3 p.f.u. (A511, A118, P40) or 5×10^6 p.f.u. (P35). Circles mark L-form (L) or walled (W) colony phenotypes. PC micrographs are shown for each colony. **f**, Infection of *E. faecalis* with phage Efs7 triggers L-form conversion. Plates were imaged at 2 d postinfection and are representative of infections at 10^3 p.f.u. **g**,**h**, *E. faecalis* L-forms retain the ability to revert to the walled state. Shown are colony morphologies at different stages of reversion (i–iv) (**g**) and corresponding PC micrographs (**h**) as observed at 2 d post infection. Figures are representative of three independent experiments (**c**–**h**). Scale bars, 0.5 mm (**c**, left; **g**), 2 µm (**c**, right; **e**,**h**).

underpinnings of endolysin-driven L-form conversion in situ and in a near-native state, we employed cryo-electron tomography (cryoET). The diameter of intact *L. monocytogenes* or *E. faecalis* cells ranges from 600 to 800 nm, which is at the upper limits of sample thickness for conventional cryoET imaging[38]. To first test whether Rev2 and *E. faecalis* cells were suitable for imaging, we used cells that were directly plunge-frozen on EM grids. The obtained tomograms revealed clear visibility of all relevant bacterial structures including the cytoplasmic membrane and peptidoglycan layer, confirming the technical feasibility of the approach (Fig. 4a,d). Next, we aimed to image L-form switching by inducing Rev2 and *E. faecalis* cells with 1 µM Ply006 or Ply007, respectively, followed by plunge freezing. Indeed, tomograms of both *L. monocytogenes* Rev2 and *E. faecalis* showed the presence of many L-form-like cytoplasmic membrane vesicles (Fig. 4c,f). Further, we observed intermediate stages of membrane protrusions extruding through punctured lesions in the peptidoglycan cell wall (Fig. 4b,e).

https://doi.org/10.1038/s41564-022-01317-3

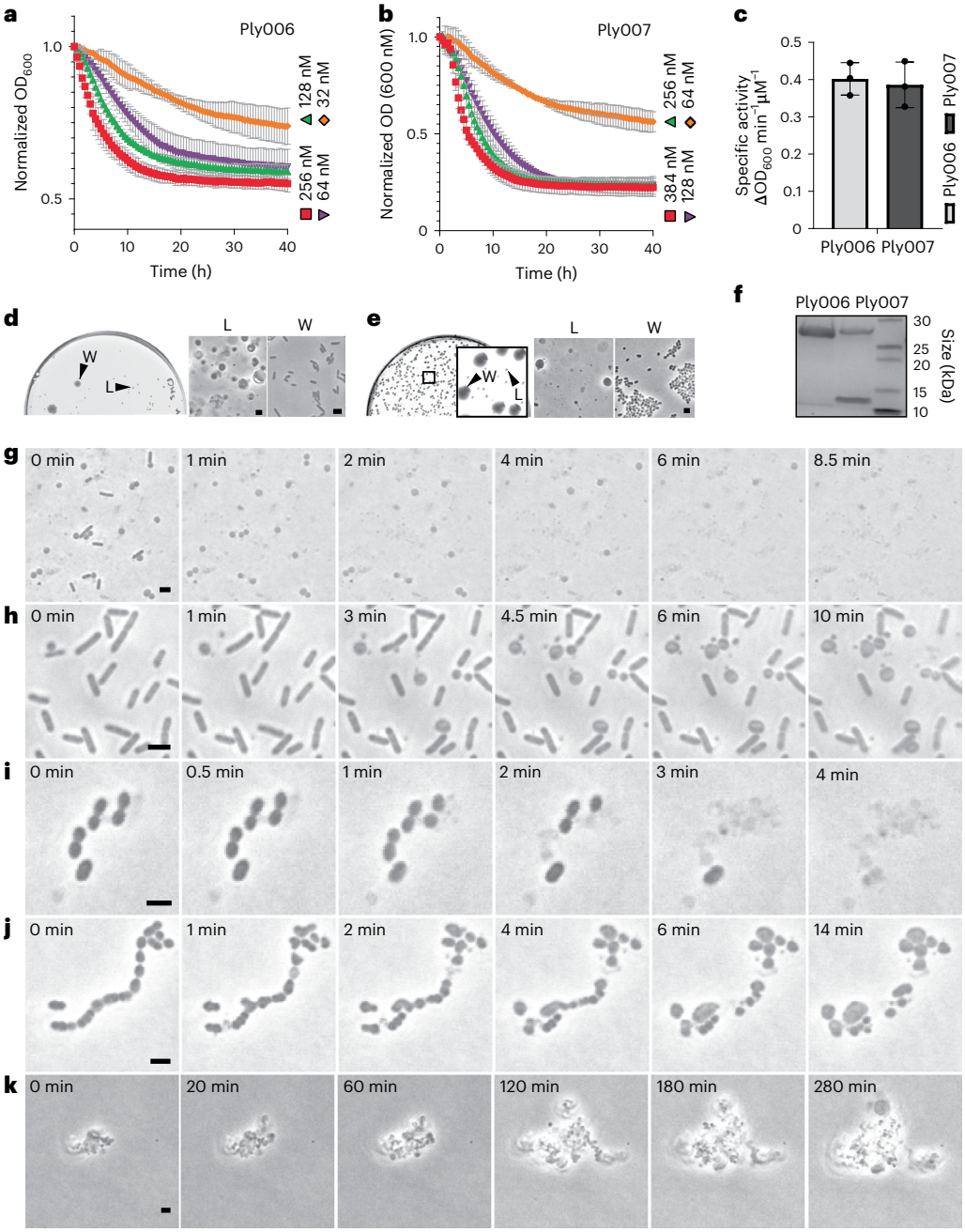

Fig. 3 | Endolysin activity promotes L-form conversion under osmoprotective conditions. a–**c**, Turbidity reduction of *L. monocytogenes* Rev2 and *E. faecalis* in liquid medium upon exposure to serial dilutions of Ply006 or Ply007, respectively (**a**,**b**) and calculation of specific enzyme activities (**c**). Specific enzyme activities of Ply006 and Ply007 (expressed as ΔOD_{600} min^{-1} μM^{-1}) were calculated from the linear activity range of the enzymes in **a** and **b**. Data are normalized to OD_{600} at $t = 0$ min, representing mean ± s.d. of three independent experiments ($n = 3$). **d** c–**e**, Endolysins trigger bacterial L-form generation. **d**, The effects of Ply006 on *L. monocytogenes* Rev2 L-form emergence. Cells were exposed to 1 μM Ply006 for 40 min. Aliquots of 50 μl were streaked on DM3 agar in 10x serial dilutions and incubated for 5 d. Shown is a plate at 10^{-4} dilution with clearly discernible walled and L-form colony morphologies (left) and corresponding PC micrographs (right). **e**, The effects of Ply007 on *E. faecalis* L-form emergence. Cells were exposed to 1 μM Ply007 for 40 min. Aliquots of 50 μl were plated on DM3 agar supplemented with 3.2 mM cysteine in 10x serial dilutions and incubated for 2 d. Shown is a plate at 10^{-3} dilution with clearly discernible walled and L-form colony morphologies (left) and corresponding PC micrographs (right). The figures are representative of at least three independent experiments (**d**,**e**). **f**, SDS–PAGE of purified Ply006, 25.7 kDa and C-terminally 6xHis-tagged Ply007 big subunit, 28.2 kDa and corresponding 6xHis-tagged small subunit, 10.01 kDa (see also Supplementary Fig. 2). Samples of 2 μg protein were loaded per lane. The uncropped version of the gel image is provided in the Source data for Fig. 3. **g**–**j**, The effects of endolysin on bacteria under hypotonic or osmoprotective conditions. *L. monocytogenes* Rev2 cells expressing chromosomally integrated eGFP or *E. faecalis* Rev cells were challenged with 1 μM Ply006 or Ply007, respectively. For time-lapse microscopy, samples were immediately transferred to standard hypotonic agar (**g**,**i**) or osmoprotective agar (**h**,**j**). Individual PC micrographs were extracted from Supplementary Videos 3, 4a, 5 and 6. **k**, Time-lapse of Ply007-induced *E. faecalis* L-form proliferation. PC micrographs were extracted from Supplementary Video 7. Scale bars, 2 μm (**d**,**e**,**g**–**k**).

https://doi.org/10.1038/s41564-022-01317-3

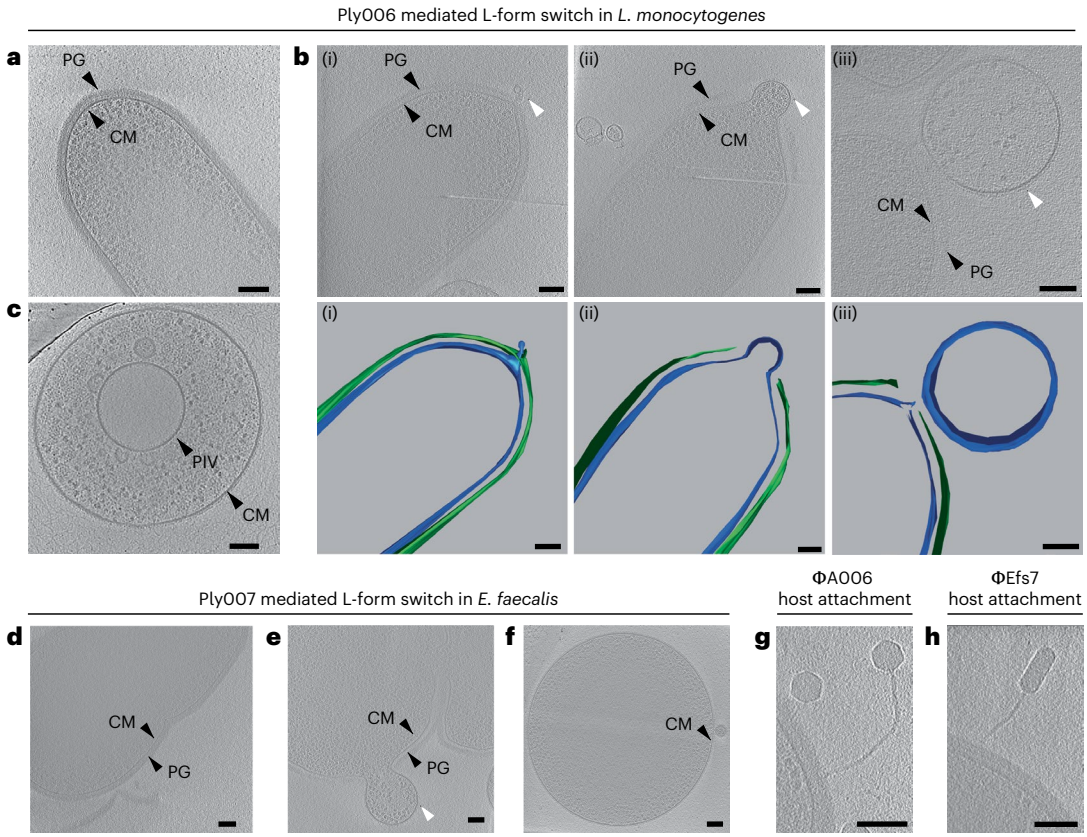

Fig. 4 | Endolysin-triggered disintegration of the cell wall induces L-form conversion. a–**c**, Cryotomograms of *L. monocytogenes* Rev2 cells revealing the effects of endolysin Ply006 exposure on the bacterial cell wall in situ. **a**, Representative Rev2 walled cell with intact cytoplasmic membrane (CM) and peptidoglycan (PG) layer. Shown is a 26-nm-thick slice through a cryotomogram. **b**,**c**, Different stages of CM blebbing (white arrows) in response to Ply006 exposure for 1 min (top) and corresponding segmented 3D model (bottom). Shown are representative images of CM extrusions emerging from different cells. CM protrudes through lesions in the peptidoglycan layer, predominantly at the cellular poles. Blebbing occurs in different stages, ranging from small membrane protrusions (i) to blebs filled with cytoplasmic content (ii) and membrane-bound L-form-like vesicles (iii). Shown are 15-nm-thick tomographic slices (green, PG; blue, CM). **c**, L-form-like vesicle completely lacking detectable PG structures. A primary internal vesicle (PIV) located within the cell is clearly visible. A 22-nm-thick tomographic slice is shown. **d**–**f**, Cryotomograms of *E. faecalis* Rev cells revealing the cell wall architecture in situ before (**d**) and after treatment with endolysin Ply007 (**e**,**f**). **d**, Dividing *E. faecalis* coccus with a distinct PG layer and CM membrane. Shown is a 28-nm-thick tomographic slice. **e**,**f**, CM blebbing and induction of L-form-like vesicles in response to Ply007 exposure. Shown are 22-nm-thick tomographic slices. **g**, Cryotomogram of an A006 virion attaching to a Rev2 host cell, 5 min post infection (bottom). Shown is an 18-nm-thick tomographic slice. **h**, Cryotomogram of an Efs7 phage attachment to an *E. faecalis* Rev host cell, 10 min post infection. A 22-nm-thick tomographic slice is shown. The micrographs are representative of at least three independent experiments (**a**–**h**). Scale bars, 100 nm. Also see Supplementary Videos 8 and 9.

On the basis of multiple tomograms of cytoplasmic extrusions that were captured at different stages, we inferred that L-form switching comprises three distinct steps. (1) First, localized enzymatic hydrolysis causes the formation of punctures in the cell wall. Small membrane protrusions begin to extrude through these holes. (2) Subsequently, the protrusions are filled with cytosolic content, driven by the internal turgor pressure of the cell. At this stage, the growing membrane bleb remains connected to the parental cell. (3) Finally, scission of the membrane bleb results in the formation of an independent and wall-deficient cell. Interestingly, we observed that Ply006-induced lesions in *L. monocytogenes* are preferentially located at the poles (Fig. 4b). This is consistent with previous studies demonstrating that cell wall binding domain of *Listeria* phage endolysin Ply006 and related enzymes preferentially attach to the polar regions of the cell wall[37,39]. Hence, it seems that the enzymatic function of Ply006 is spatially guided by its CBD. In contrast, no such site specificity was observed for the *Enterococcus* phage endolysin Ply007.

Phage-infected cells are no longer capable of L-form escape

The above results suggested that phage-induced L-form conversion is triggered by endolysins. However, we had no means of directly assessing whether this phenomenon occurred primarily with non-infected bystanders (lysis-from-without), or possibly also as a result of phage infection (lysis-from-within). Employing a synthetic phage engineering platform[24], we created an A006-based reporter phage expressing a fluorescent protein, allowing direct monitoring of infected cells. To obtain high expression levels, a modified *gfp* gene was inserted and placed under control of the strong A006 major capsid protein promoter P_{cps}[30,32]. The strategy for the design of corresponding genome fragments for phage assembly is shown in Fig. 5a,b, followed by rebooting in L-form cells[24]. Correct genome sequence was confirmed by DNA sequencing. Plaque phenotypes and phage concentration-dependent host killing were validated using soft agar overlay assays (Fig. 5c,d) and lysis kinetics monitored in liquid culture (Fig. 5e). As expected, engineered A006::*egfp*$_{cps}$ showed similar lysis characteristics as the wild type, and phage-induced eGFP production became detectable at 45 min after infection (Fig. 5g). If L-form conversion of phage-infected cells were possible, infection with A006:*egfp*$_{cps}$ would result in eGFP labelled *L. monocytogenes* cells, visible even after L-form conversion. To test this, we infected Rev2 walled cells expressing chromosomally integrated RFP (red fluorescent protein) with excess amounts of A006::*egfp*$_{cps}$, resulting in transient eGFP

https://doi.org/10.1038/s41564-022-01317-3

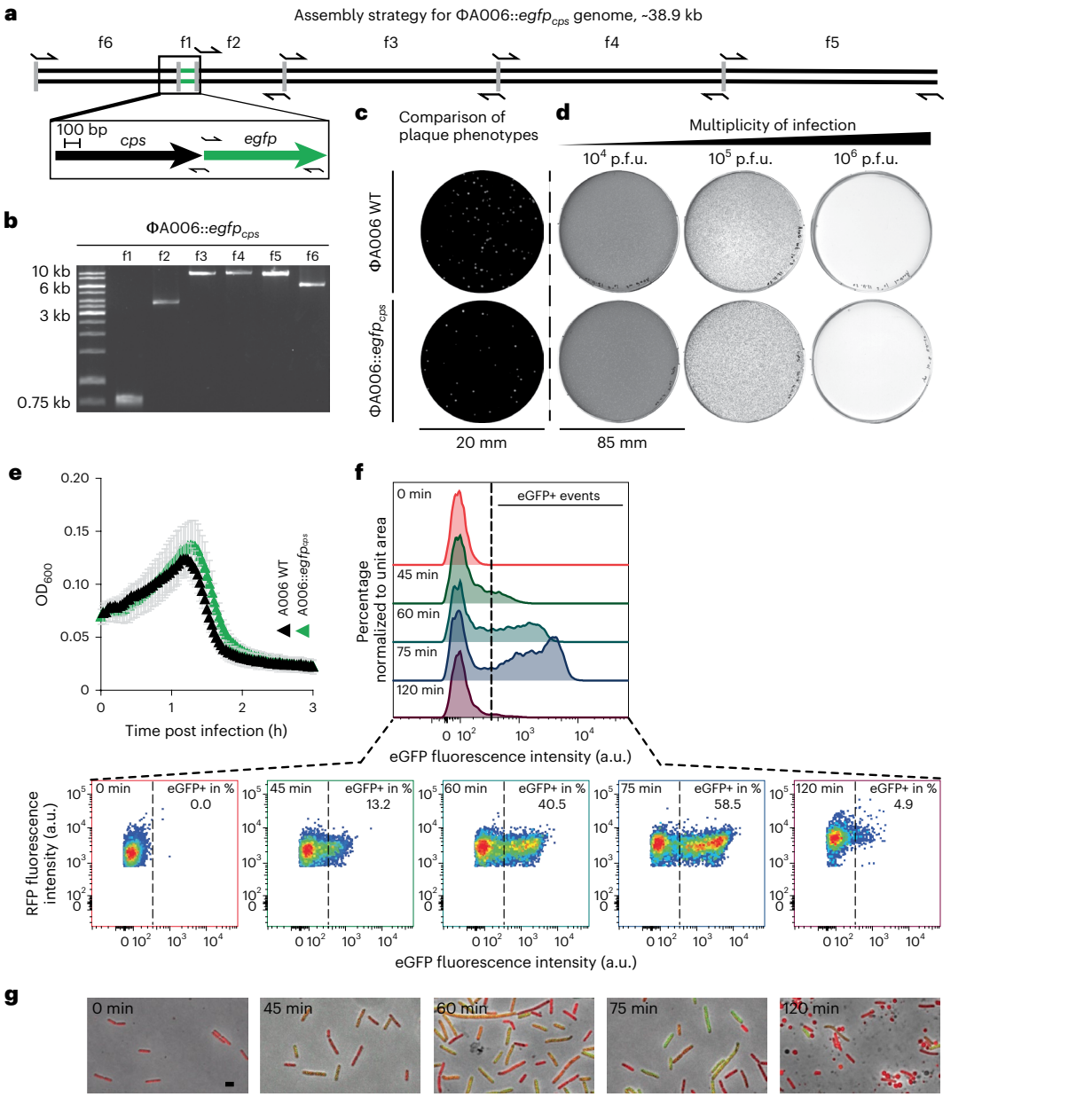

Fig. 5 | Bacterial cells undergoing productive phage infection do not form stable vesicles or wall-deficient L-form cells. a,**b**, Engineering of a phage that allows fluorescence-based single-cell tracking of productive phage infection in *L. monocytogenes*. Strategy for synthetic assembly of phage A006::*egfp*$_{cps}$ (**a**) where *gfp* is placed under the control of the major capsid protein gene *cps* promoter, expression of which indicates productive phage infection. Arrows denote primer binding sites for PCR amplicons f1–f6 (**b**). **c**, Comparison of plaque phenotypes between wild-type (WT) phage A006 and A006::*egfp*$_{cps}$ as observed on soft agar overlay plates. Shown are representative plaque phenotypes at 24 h post infection, using *L. monocytogenes* Rev2 as a host (**c**,**d**). **d**, Concentration-dependent host killing in plate culture where phage A006 and its mutants were titrated in 10-fold serial dilutions. **e**, Comparison of host killing kinetics in liquid infection (left) and corresponding fluorescence emission intensities (right). *L. monocytogenes* Rev2 bacteria were challenged with excess amounts of A006 or A006::*egfp*$_{cps}$ in DM3$_{\Phi}$ liquid medium. Turbidity or fluorescence intensity was monitored for 3 h. Data are displayed as mean ± s.d. of three independent experiments ($n = 3$). **f**, Flow cytometry analysis of *L. monocytogenes* Rev2 cells expressing chromosomally integrated RFP upon infection with excess amounts of A006::*egfp*$_{cps}$ in DM3$_{\Phi}$ medium. Fluorescence-positive events (eGFP+) represent infected cells undergoing productive phage infection. Samples were analysed at 0, 45, 60, 75 or 120 min post infection. Overlayed histograms depict eGFP fluorescence intensity (arbitrary units, a.u.) vs percentage of cells normalized to the mode. Pseudocolour density plots show eGFP fluorescence intensity (a.u.) vs RFP fluorescence intensity (a.u.) displayed on a biexponential scale. The threshold value for eGFP+ events was set to 400 a.u. (dashed black line). Data are representative of three independent biological experiments. **g**, Micrographs of bacterial cells taken from **f**. Shown are merged images of channels for green and red-light emission and PC channel. Walled bacterial cells undergo a 'green-shift' due to transient phage-encoded GFP fluorescence. L-form switching occurs between $t = 75$ min and $t = 120$ min post infection. Note that wall-deficient cells ($t = 120$ min) express RFP but not eGFP. Scale bar, 2 µm.

fluorescence in the majority of walled cells (Fig. 5f,g and Supplementary Fig. 3). Eventually, phage-induced lysis caused a sharp decrease in fluorescence due to explosive cell death by sudden osmotic lysis of virtually all infected cells. In contrast, the red-fluorescent RFP-expressing cells showed massive L-form switching instead of complete lysis. In conclusion, these results strongly suggest that the non-infected bystander cells are responsible for L-form generation, not the phage-infected bacteria.

https://doi.org/10.1038/s41564-022-01317-3

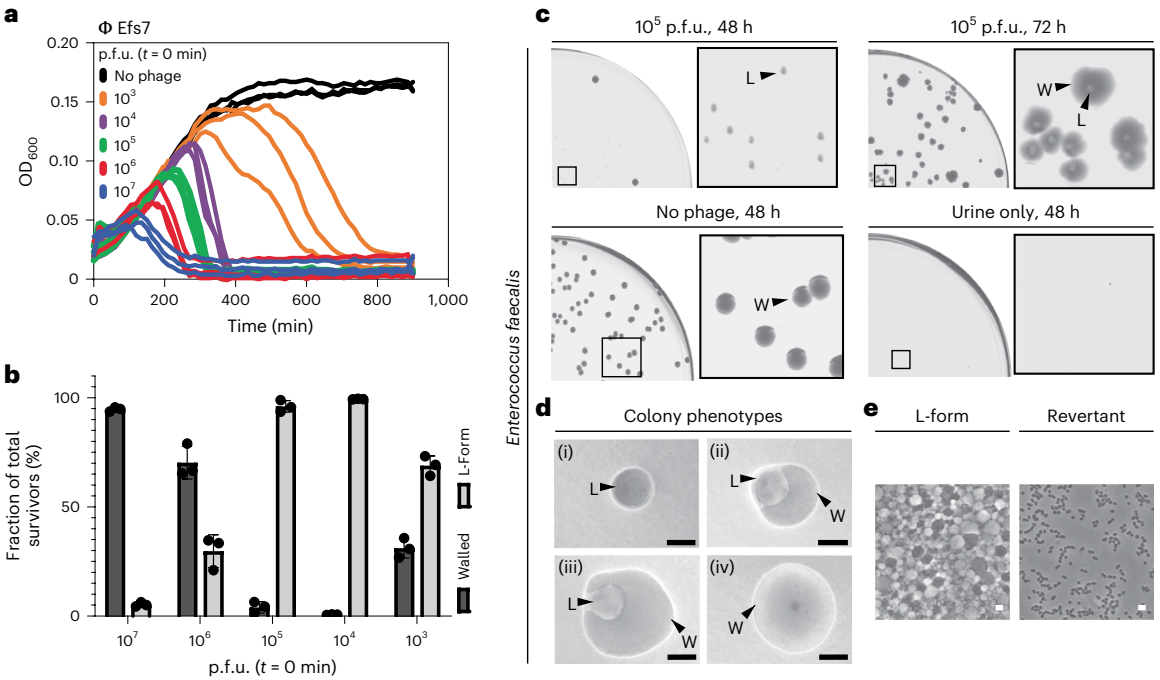

Fig. 6 | Phage-induced *E. faecalis* L-form conversion in human urine. a–**c**, Phage Efs7 infection of *E. faecalis* in human urine triggers L-form generation. **a**, Growth curves in human urine for *E. faecalis*. Bacteria were challenged with serial dilutions of phage (10^7, 10^6, 10^5, 10^4, 10^3 p.f.u.) or no phage at $t = 0$ min. As a control, sterile-filtered urine was incubated without bacteria (shown in **c** only). For each condition, three independent replicates are presented as individual curves. **b**,**c**, Relative quantification of L-form survival after phage infection. Cultures from **a** were plated 15 h after infection on DM3 supplemented with cysteine. Populations of L-forms and walled survivors are normalized to the total c.f.u. per infection. Quantification was performed at 48 h after streaking. Data are mean ± s.d. of three independent experiments ($n = 3$). **c**–**e**, Effect of phage infection in human urine on L-form emergence and reversion. **c**, Representative high-resolution plate scans obtained from **b**. Top panel shows identical streaks of *E. faecalis* at 48 h and 72 h after Efs7 infection with 10^5 p.f.u. Note that after 48 h, all colonies show the L-form phenotype (L), followed by reversion back to the walled state (W) after 72 h. Bottom panels show controls of *E. faecalis* with no phage or sterile-filtered urine only after 48 h incubation. **d**,**e**, Individual colony phenotypes observed in **c**. Micrographs show *E. faecalis* L-form colonies (i), intermediate states of reversion (ii,iii) and walled cells (iv). Corresponding PC micrographs show cell morphology. The figures are representative of at least three independent experiments. Scale bars, 0.5 mm (**d**), 2 µm (**e**).

Loss of wall teichoic acids mediates phage resistance

Phage infection of Gram-positive bacteria requires cell wall-associated binding ligands, such as wall teichoic acids covalently linked to the peptidoglycan of the host[2–4]. For example, the A006 receptor binding protein A006_gp17 is known to recognize specific sugar decorations of wall teichoic acids with high selectivity and sensitivity[40]. Because L-form conversion leads to a complete loss of the cell wall-associated phage receptors, it seemed reasonable to assume that L-forms are resistant to phage infection via this route. This idea was also supported by the massive emergence of L-forms observed here (Fig. 2). To provide formal proof, we exposed *L. monocytogenes* Rev2 L-forms expressing chromosomally integrated RFP to excess amounts of A006::$egfp_{cps}$. Indeed, microscopic analysis revealed complete absence of fluorescence in L-forms even after prolonged periods of incubation, indicating that L-forms are not supporting phage binding and subsequent genome injection (Supplementary Fig. 4) due to a lack of wall teichoic acid ligands.

Phage-induced L-form cells in human urine

On the basis of our observation of phage-induced L-form switching, we asked whether this process may also be relevant under conditions found in a natural environment. Phage therapy is currently developed as a treatment option for several pathogens causing urinary tract infections, including *E. faecalis*[41–43]. It has recently been shown that urine provides the necessary osmoprotection to enable L-form switching and survival[17]. We therefore asked whether phage Efs7 infection of *E. faecalis* in human urine would potentially also result in L-form conversion. To test this hypothesis, we challenged the bacteria with serial dilutions of Efs7 in sterile-filtered human urine, followed by incubation overnight (Fig. 6a), plating and quantification of the fraction of walled survivors and L-forms after 2 d (Fig. 6b–e). Strikingly, we found that Efs7 indeed induced a massive induction of L-forms in urine. In line with the results obtained for *L. monocytogenes*, excess amounts of phage reduce the fraction of L-form survivors after infection, whereas lower phage concentrations were more effective and resulted in L-forms being the vast majority of bacterial survivors (Fig. 6b,c). Notably, almost all *E. faecalis* L-form colonies were able to undergo reversion to the walled state within 72 h (Fig. 6c).

Discussion

In the lytic cycle, phage infection normally results in sudden lysis of the host, at least under standard culture conditions that are generally hypotonic. Here we report that in an osmoprotective environment, Gram-positive bacteria such as *L. monocytogenes* or *E. faecalis* can evade phage-induced lysis by transiently switching to a wall-deficient L-form state that confers resistance to phage infection. Our results show that the conversion to the L-form occurs due to collateral damage to the bacterial cell wall caused by the release of phage endolysins during the lytic cycle. Consequently, this effect can contribute to transient persistence and rescue of viability of bacterial communities by enabling L-form conversion of uninfected cells before phage infection is initiated. On the basis of our experiments with phage endolysins Ply006 and Ply007, we propose a mechanistic model of L-form escape that comprises three major steps: (1) endolysin-mediated induction of punctured lesions in the cell wall and extrusion of small membrane protrusions, (2) maturation, that is, turgor-driven filling of the wall-deficient cell with cytosolic

content including genomic DNA and (3) scission of cell membranes to form independent and viable L-form cells (Supplementary Fig. 5).

Given that expression of endolysins at the end of the lytic cycle is a shared feature of all tailed phages, it is likely that phage-induced L-form escape occurs among a wider range of Gram-positive bacteria, especially during growth in confined environments. This hypothesis is supported by our observation that L-form escape can be induced by different phages, including temperate and virulent members of the *Siphoviridae* and *Myoviridae*. Importantly, loss of the cell wall confers resistance of L-forms against viral infection due to the lack of cell wall-associated phage receptors, such as wall teichoic acids, and seems pivotal for L-form survival. Blocking or loss of phage receptors is a common strategy for bacteria to acquire transient or permanent resistance to phage infection[44,45]. Typically, these evasion mechanisms involve the modification of binding ligands or conformational changes of the cell surface[3]. In contrast, the phenomenon observed here is unique in that it results in a complete loss of peptidoglycan, including cell surface structures that represent potential receptors. However, it is important to note that phage-induced L-form cells are only transiently wall-deficient and can revert to the walled state in the absence of selective pressure. Therefore, this route can serve as a self-sustaining evasion mechanism to escape phage killing. Indeed, the massive emergence of L-forms following phage exposure indicates that endolysin-mediated L-form release is frequent and widespread, rather than an exceptional and singular event. Notably, due to very rapid enzyme kinetics, endolysin-mediated generation of L-forms occurs within seconds. Because bacteria often exist in dense communities, it is conceivable that endolysins released during lysis of phage-infected bacteria act on neighbouring cells even before they may be infected by progeny phage. This is consistent with our observation that the fraction of L-form survivors increases at lower phage concentration. Thus, under such circumstances, the L-form state may offer a physiological refuge that aids bacterial survival. Remarkably, the effect was also observed for uropathogenic *E. faecalis* in human urine as a suitable ex vivo environment, providing strong evidence that phage-induced L-form switching occurs during phage exposure of bacterial communities under natural conditions. Even though the impact and possible roles of L-forms in the environment remains elusive, nature provides a multitude of ecological niches that should in principle allow L-form growth. Notably, L-forms have been previously reported to occur in a range of natural sources, including samples obtained from plants, animals and humans[16,18]. Further, some evidence exists that bacterial wall deficiency may also be triggered within infected eukaryotic cells[14,46]. Importantly, L-forms appear to be frequently present in clinical urine samples of elderly patients[17]. The phage–bacteria interactions uncovered in this study, particularly endolysin-triggered L-form escape and subsequent reversion, could have important implications for future efforts in phage- and endolysin-based therapeutic interventions. Indeed, L-form formation in Gram-positive pathogens as a result of such treatments may represent a previously overlooked source of bacterial survival and persistence and may therefore be of particular importance. This emphasizes the need for application of additional effectors beyond the cell wall lytic activity of peptidoglycan hydrolases or phages, such as a combination treatment with non-cell wall targeting drugs and antibiotics.

Methods

Bacterial strains and growth conditions

Bacterial strains used in this study are listed in Supplementary Table 1. Half-strength (0.5x) brain-heart infusion medium (BHI, Biolife Italiana) was used as a standard hypotonic medium for growth of *L. monocytogenes* and BHI-FC (37 g l^{-1} BHI, 4 g l^{-1} glycine, 6.06 g l^{-1} Tris, pH 7.5) was used as standard hypotonic medium for growth of *E. faecalis* at 30 °C. L-forms were induced and grown in osmoprotective modified DM3 liquid medium, referred to as $DM3_{\Phi}$ (5 g l^{-1} tryptone, 5 g l^{-1} yeast extract, 0.01% BSA, 125 mM succinic acid, 180 mM glucose, 20 mM K_2HPO_4, 11 mM KH_2PO_4, 20 mM $MgCl_2$, 200 uM $CaCl_2$, pH 7.3), at 30 °C. DM3 agar (5 g l^{-1} tryptone, 5 g l^{-1} yeast extract, 0.01% BSA, 500 mM succinic acid, 180 mM glucose, 20 mM K_2HPO_4, 11 mM KH_2PO_4, 20 mM $MgCl_2$, pH 7.3)[47] was used for L-form growth on plate. For *E. faecalis* L-forms, $DM3_{\Phi}$ liquid medium and DM3 agar were supplemented with 3.2 mM L-cysteine. Microaerophilic conditions for growth in plate culture were generated using microaerophilic atmosphere generation bags (BioMerieux) in an anaerobic jar. *Escherichia coli (E. coli)* strains XL1 Blue MRF' and BL21 Gold (DE3) were grown in LB medium (10 g l^{-1} tryptone, 5 g l^{-1} yeast extract, 5 g l^{-1} NaCl) at 37 °C. If required, antibiotics were added at the following concentrations: ampicillin 50 µg ml^{-1}, chloramphenicol 10 µg ml^{-1}, erythromycin 5 µg ml^{-1}.

DNA manipulation and cloning procedures

Isolation of plasmid DNA and transformation into *E. coli* or Rev2 were conducted according to standard procedures[28,48,49]. For subcloning of plasmid pET302/*ply006*, purified pET302 vector (Invitrogen) and codon optimized synthetic DNA (Gene Art DNA Strings, Thermo Fisher) encoding *ply006* gene and appropriate restriction sites were digested using restriction enzymes NdeI and BamHI-HF (New England Biolabs), followed by ligation with T4 DNA ligase (Thermo Fisher) and transformation into *E. coli* BL21 Gold (DE3). Sequence identity was confirmed by Sanger sequencing (Microsynth). For subcloning of pET21a/*ply007*, the backbone of pET21a (EMD Biosciences) was amplified using primers JPR1168 and JPR1169. *Ply007* was amplified using primers JPR1170 and JPR1171. Individual fragments were assembled by Gibson assembly at 50 °C for 1 h in a total reaction volume of 20 µl (NEBuilder HiFi DNA Assembly Cloning kit, New England Biolabs), fusing 6xHis-tag coding sequences to the 3' end of *ply007*. Resources used in this study are disclosed in Supplementary Tables 1 and 2.

Phage propagation and purification

The soft agar overlay method was employed for phage propagation using LC soft agar (0.4% LB agar, 10 mM $MgSO_4$, 10 g l^{-1} glucose; supplemented with 10 mM $CaCl_2$) as top agar and 0.5 BHI agar for plating. Phages and propagation hosts are listed in Supplementary Table 1. For extraction, semi-confluent plates were incubated with 3 ml SM buffer (100 mM NaCl, 8 mM $MgSO_4$ and 50 mM Tris, pH 7.4), followed by 0.2 µm sterile filtration of the suspension. All crude lysates were treated with DNAse I (10 µg ml^{-1}) and RNAse (1U per 10 ml) for 1 h at 37 °C. For precipitation, one volume of precipitation solution (polyethylene glycol (PEG), 3 M NaCl, 30% PEG8000) was added to two volumes of lysate and incubated on ice for 24 h, followed by centrifugation at 10,000 × *g* for 15 min at 4 °C. Pellets were resuspended in 5 ml SM buffer and purified via CsCl density gradient ultracentrifugation (Optima XPN-80 ultracentrifuge; Beckman Coulter) at 19,200 × *g* for 18 h at 10 °C. Purified phage bands were carefully isolated using a syringe, dialysed two times against 1000x excess of SM buffer and stored at 4 °C.

Assembly of synthetic genomes, L-form transformation and genome rebooting

Assembly, transformation and rebooting of synthetic bacteriophage genomes were performed as described earlier[24] with slight modifications. Bacteriophage genomes were designed in silico; resources are listed in Supplementary Table 3. Briefly, codon optimized e*gfp* and a strong ribosomal binding site (RBS, GAGGAGGTAAATATAT) sequence were inserted downstream of gene *cps* (*gp07)*. Designed fragments were PCR-amplified from purified phage A006 or synthetic DNA to yield a total of six DNA fragments (f1–f6) per phage genome, followed by Gibson assembly at 50 °C for 1 h in a total reaction volume of 20 µl (NEBuilder HiFi DNA Assembly Cloning kit, New England Biolabs). Assembly reactions were carried out with purified DNA fragments to yield synthetic genomes. For L-form transfection, *L. monocytogenes* Rev2 was used for rebooting[24]. To this end, 5 µl of a frozen stock was

inoculated in DM3 medium and incubated statically at 32 °C for 24 h. The culture was adjusted to optical density $(OD)_{600\,nm}$ = 0.15. For L-form transfection, 100 µl of adjusted L-form culture was mixed thoroughly with 150 µl heat-sterilized 40% PEG8000 and 20 µl of Gibson assembly reaction in 50 ml falcon tubes using wide-bore pipette tips. After 5 min, 10 ml of prewarmed DM3 medium was added to the mix and incubated at 32 °C for 8 h. Matured phage particles were detected by the soft agar overlay method, followed by screening for plaques. To this end, 5 ml of molten LC soft agar was mixed with 50 µl of transfected L-forms and 200 µl of an EGD-e overnight culture, plated on 0.5 BHI agar plates and incubated at room temperature. Individual plaques were picked after 24 h and propagated three times. For visualization, plates were scanned in transillumination mode (Image Scanner, Amersham Biosciences); contrast was adjusted for clarity where necessary.

Time-course turbidity or fluorescence assays

Time-course turbidity assays were performed for wild-type phage A006 and A006::$egfp_{cps}$ to demonstrate that the lysis kinetics of both phages are comparable. To this end, mid-exponential *L. monocytogenes* Rev2 cells expressing chromosomally integrated RFP were pelleted at 12,000 × *g* for 4 min, resuspended in $DM3_{\Phi}$ and adjusted to OD_{600} of 0.1 (≈10^8 bacteria per ml). Diluted culture (190 µl) was infected with 10 µl of A006 or A006::$egfp_{cps}$ phage lysate (10^{10} p.f.u. ml^{-1}(plaque forming units)). Turbidity was monitored at 2 min intervals at 30 °C in flat-bottom 96-well plates using a FLUOstar OMEGA plate reader (BMG LABTECH). Plates were agitated before each measurement. Identical infection conditions were used for fluorescence time-course assays. Fluorescence intensities were measured in black-walled 96-well plates with a FLUOstar OMEGA plate reader (BMG LABTECH) at 485 nm excitation wavelength with a 520 nm emission filter. Fluorescence time-course assays were background corrected by subtraction of controls (bacteria+ phage A006). All data were acquired using OMEGA software v5.10 in three independent experiments.

Phage adsorption assay

To quantify A006 phage adsorption to the bacterial surface, overnight cultures of *L. monocytogenes* EGD-e or mutants EGD-e *Δlmo1083* (rhamnose-deficient) or EGD-e *Δlmo2550* (GlcNAc-deficient), phage pulldown assays were performed as previously described[2]. The number of adsorbed phage particles was determined by plaque assays using the soft agar overlay method.

Phage survival assay

To quantify L-form induction and survival in response to phage infection, overnight cultures were diluted 1:20 with 0.5 BHI or BHI-FC and grown to mid-exponential phase. Bacteria were pelleted at 12,000 × *g* for 4 min and resuspended in $DM3_{\Phi}$ medium or sterile-filtered human urine and adjusted to OD_{600} = 0.0375. Decimal serial dilutions of purified phage were prepared, and 10 µl of each dilution were added to 190 µl of cell suspension, followed by incubation in flat-bottom 96-well plates at 30 °C using a FLUOstar OMEGA plate reader (BMG LABTECH). To follow phage-induced bacterial lysis over time, OD_{600} was monitored at 5 min intervals, and plates were agitated before each measurement. To quantify L-form survival, serial dilutions of individual infections were plated on osmoprotective agar. Viable L-form and walled bacterial counts were enumerated at 2–5 d post infection. Data were acquired in three independent experiments and three technical replicates per experiment. Ability of L-form colonies to revert in the absence of phage was tested by picking and inoculation of L-form cells on DM3 agar. Reversion (that is, occurrence of walled cells) was confirmed by light microscopy.

Endolysin overexpression and purification

Codon optimized endolysin Ply006 was expressed from vector pET302; C-terminally 6xHis-tagged Ply007 was expressed from vector pet21a(+) in *E. coli* BL21 Gold (DE3) cells in LB-PE medium (15 g l^{-1} tryptone, 8 g l^{-1} yeast extract, 5 g l^{-1} NaCl, pH 7.8)[50]. Recombinant protein expression was induced with 0.5 mM isopropyl-β-D-1-thiogalactopyranoside (IPTG) at mid-exponential phase and allowed to proceed for 18 h at 19 °C. Bacteria were collected by centrifugation at 7,000 × *g* for 10 min at 4 °C, lysed in buffer A (20 mM Na_2HPO_4, 30% glycerol, pH 7.4) using a Stansted Fluid Power pressure cell homogenizer (100 MPa) and centrifuged at 20,000 × *g* for 60 min at 4 °C to remove cellular debris. Cleared lysates containing proteins with no His tag were purified by cation exchange chromatography using a 5 ml HiTrap Sepharose SP FF column (GE Healthcare) fitted on an ÄKTA fast protein liquid chromatography device (GE Healthcare). After washing, bound proteins were eluted with buffer B (20 mM Na_2HPO_4,1 M NaCl, 10% glycerol, pH 7.4). Proteins (6xHis-tagged) were purified by immobilized metal ion chromatography using nickel-NTA super flow resin (Qiagen) as previously described with slight modifications[51]. Briefly, the column was washed with 25 column volumes of lysis buffer (50 mM Na_2HPO_4, 300 mM NaCl, 10 mM imidazole, 30% glycerol, pH 8.0), followed by elution of target proteins with elution buffer (50 mM Na_2HPO_4, 300 mM NaCl, 250 mM imidazole, 30% Glycerol, pH 8.0) in 1 ml fractions. All purified proteins were dialysed against 1000x excess of dialysis buffer (30% glycerol, 50 mM NaH_2PO_4, 300 mM NaCl, pH 7.5). Protein identity was confirmed by SDS–PAGE using Mini-Protean TGX-stain-free precast gels (Bio-Rad). Concentration was measured using a Nanodrop ND-1000 spectrophotometer (Thermo Fisher).

Endolysin catalytic activity and L-form survival assay

To assess the specific activity of Ply006 on *L. monocytogenes* strain Rev2 and Ply007 on *E. faecalis*, turbidity reduction of bacterial substrate cells was measured at 600 nm in flat-bottom 96-well plates using a FLUOstar OMEGA plate reader (BMG LABTECH). Briefly, cultures of *L. monocytogenes* strain Rev2 or *E. faecalis* were diluted to OD_{600} of 0.1 in 0.5 BHI or BHI-FC, respectively, and incubated until reaching mid-exponential phase. Cells were pelleted by centrifugation at 8,000 × *g* for 5 min and resuspended in $DM3_{\Phi}$ or $DM3_{\Phi}$ supplemented with 3.2 mM L-cysteine, respectively, to reach a final OD_{600} of 2. To determine the linear activity range, 2x serial dilutions of purified endolysin were prepared and 100 µl of each dilution were mixed with 100 µl of the corresponding cell suspension. Turbidity reduction was monitored at 5 min intervals at 30 °C for 40 min. Plates were agitated before each measurement, and lysis curves were blank corrected against medium without endolysin and bacteria. To determine specific enzyme activities, lysis curves were fitted to a 5-parametric sigmoidal function using SigmaPlot 13 (Systat software) as described previously[52]. The steepest slopes of individual lysis curves within the linear activity range were used to calculate the specific activities in Excel (Microsoft) as described earlier[51]. All data were acquired in three independent experiments from technical triplicates.

Mass spectrometry

Protein masses were identified using liquid chromatography-electrospray ionization-mass spectrometry (LC-ESI-MS) at the Functional Genomics Center Zürich, Switzerland (www.FGCZ.ch), using standard protocols. Briefly, before ESI-MS analysis, the sample was desalted using a C4 ZipTip (Millipore) and analysed in MeOH:2-PrOH:0.2% FA (30:20:50). The solution was infused through a fused silica capillary (ID 75 µm) at a flow rate of 1 µl min^{-1} and sprayed through a PicoTip (ID 30 µm, New Objective). Nano ESI-MS analysis of the samples was performed on a Synapt G2_Si mass spectrometer and the data were recorded with the MassLynx 4.2 software (Waters). Mass spectra were acquired in the positive-ion mode by scanning an *m*/*z* range of 400–4,000 Da with a scan duration of 1 s and an interscan delay of 0.1 s. The spray voltage was set to 3 kV, the cone voltage to 50 V and the source temperature to 80 °C. For every detected species, the recorded m/z data were individually deconvoluted into mass spectra by applying the maximum entropy algorithm MaxEnt1 (MaxLynx),

with a resolution of the output mass at 0.5 Da per channel and uniform Gaussian damage model at the half height of 0.7 Da.

Microscopic imaging

Light microscopy and confocal laser scanning microscopy was performed using an inverted Leica TCS SPE research microscope (Leica Microsystems) with an HCX PL FLUOTAR 100.0 × 1.30 oil objective, DFC360 FX camera and Leica application suite software v2.5.1.6757 fitted with an environmental chamber. For snapshot live-cell imaging, *L. monocytogenes* samples were mounted on microscopic slides covered with 1% 0.5 BHI agar or 1% DM3 agar for L-forms; *E. faecalis* samples were mounted on 1% BHI-FC agar or 1% DM3 agar supplemented with 3.2 mM L-cysteine for L-forms. To avoid drying of the agar film, cover slips were sealed using transparent nail polish. All time-lapse imaging was performed at 30 °C. Where appropriate, fluorescence channels were included using an excitation wavelength of 488 nm for eGFP-expressing samples and 532 nm for RFP-expressing samples. For time-lapse imaging of A006 ΔLCR-mediated L-form switching, exponential cultures of Rev2 cells expressing chromosomally integrated eGFP were pelleted and OD was adjusted to 0.0375 (≈3.75×10^7 bacteria per ml) with $DM3_{\Phi}$. Diluted culture (190 µl) was infected with 10 µl of A006 ΔLCR phage lysate (5×10^5 p.f.u. ml^{-1}) at 30 °C. Time-lapse imaging was started at 6 h post infection. To observe L-form proliferation, time-lapse imaging was started at 18 h post infection. For snapshot imaging of A006-mediated effects on L-form switching, Rev2 cells were pelleted, and OD_{600} was adjusted to 0.0375 using $DM3_{\Phi}$ or 0.5 BHI, followed by infection with 10 µl of A006 phage lysate (5×10^5 p.f.u. ml^{-1} or 5×10^6 p.f.u. ml^{-1}) at 30 °C. Bacterial growth and lysis were monitored spectrophotometrically as described above and samples were imaged at several timepoints throughout the infection process. For snapshot imaging of L-forms in the presence of phage, Rev2 L-form cultures expressing RFP were adjusted to an OD_{600} of 0.2. Bacterial cultures (190 µl) were mixed with 10 µl of A006::$egfp_{cps}$ (10^{10} p.f.u. ml^{-1}). Samples were imaged after 0, 45, 60, 75 or 120 min. For time-lapse imaging of endolysin-treated bacteria under hypotonic or osmoprotective conditions, mid-exponential bacterial culture was pelleted and resuspended with appropriate purified endolysin to reach a final concentration of 1,024 nM and an OD_{600} of 1. Samples were immediately mounted for microscopy. To observe endolysin-induced L-form emergence, bacteria were exposed to endolysin for 1 h at 30 °C, followed by time-lapse imaging. Low-magnification imaging of bacterial colonies was performed using a Leica S6 D stereomicroscope equipped with an MC 170 HD camera. Image analysis and processing were performed using Fiji v1.51 (National Institutes of Health).

Plunge freezing

Plunge freezing was performed using an FEI Vitrobot (Thermo Fisher)[53]. For cryoET sample preparation of bacterial cells, 10 nm colloidal gold fiducial markers (Sigma-Aldrich) were added to each sample at a ratio of 1:5 (v/v) to allow tilt image alignments. For Vitrobot setup, a filter paper (Whatman, 47 mm diameter) and a Teflon sheet were installed for single-sided blotting in a pre-cooled chamber (4 °C) with 100% humidity. EM grids (R2/2, Cu 200 mesh; Quantifoil Micro Tools) were glow-discharged for 45 s at 25 mA by PELCO easiGlow discharger. Sample aliquots (4 µl) were applied to each grid, incubated for 15 s and blotted for 6.5 s, followed by immediate plunge freezing in an ethane:propane mixture (37% v/v ethane:63% v/v propane)[54]. Grids were stored in liquid nitrogen. Before loading of the samples into the cryo-electron microscope, the grids were clipped. For sample preparation, all bacterial samples were pelleted, and OD_{600} was adjusted to 2–2.5 before blotting. If required, *L. monocytogenes* or *E. faecalis* cells were exposed to 1,024 nM purified Ply006 or Ply007, respectively, followed by plunge freezing at the desired timepoints. For imaging of phage adsorption, bacterial cultures were adjusted to an OD_{600} of 0.1. Samples (95 µl) were then mixed with 5 µl of purified phage lysate (10^{11} p.f.u. ml^{-1}), followed by 5 min incubation at room temperature.

CryoET

For cryoET imaging, all tilt series images were collected in a Titan Krios 300 kV transmission electron microscope (Thermo Fisher) equipped with a field emission gun, an energy filter (slit width 20 eV; Gatan) and K2 or K3 direct electron detectors (Gatan). Images were recorded at a pixel size of 4.34, 2.68 or 3.4 Å. Tilt series were collected from −60° to +60° with 2° increments and a defocus of −9 µm. A cumulative total dose of 120–150 $e^- Å^{-2}$ was used for acquisition. Tilt series and two-dimensional images were automatically acquired using SerialEM 3.7[55].

Tomogram reconstruction

Drift-correction and exposure-filtering was conducted using Alignframes. Three-dimensional reconstructions and segmentations were calculated using IMOD software package[56,57]; where appropriate, deconvolution filtering was employed. Visualization and two-dimensional slices through a three-dimensional volume were acquired using 3dmod.

Flow cytometry analysis

Flow cytometry was performed on a BD FACS Aria III cell sorting device equipped with BD FACS Diva 8.01 software (BD Biosciences). Before experiments, voltage settings for the relevant fluorescence channels were adjusted by running *L. monocytogenes* strain Rev2 walled cells expressing no fluorescent proteins or eGFP or RFP. Fluorescence was measured after excitation at 488 nm (eGFP) or 561 nm (RFP) using 530/30 nm and 610/20 nm bandpass filter, respectively. Forward scatter (FSC-H) and side scatter (SSC-H) threshold values were set to 500 to minimize noise. For all experiments, bacterial cells expressing chromosomally integrated RFP were used. Bacterial events were identified on the basis of scatter (FSC-H) and RFP fluorescence intensity (Supplementary Fig. 3). To eliminate doublets, serial dilutions of bacteria were run to determine the linear range of the event rate. Flow cytometry-grade PBS (pH 7.4, Thermo Fisher) was used as sheath fluid. For analysis of phage-induced eGFP fluorescence, mid-exponential *L. monocytogenes* strain Rev2 cells expressing RFP cells were diluted to an OD_{600} of 0.1. Diluted samples (190 µl) were infected with 10 µl A006::$egfp_{cps}$ (10^8 p.f.u.) at 30 °C. Samples were incubated for 45, 60, 75 or 120 min and diluted 1:50 in flow cytometry-grade PBS (pH 7.4). Diluted samples were immediately analysed from a 1.5 ml tube with no swirling at 4 °C. The flow was adjusted to the lowest flow rate (~12 µl min^{-1}), resulting in 200–500 events per second. For each sample, 10,000 events were measured. All FACS analysis was complemented by simultaneous microscopic analysis of each sample (see Microscopic Imaging section). Selected samples were chosen for reanalysis as a quality control. To this end, cell sorting was performed using a 70 µm nozzle at 87 kHz. The drop delay was set manually using BD FACS Accudrop beads (BD Biosciences) before the experiment. Samples were acquired at the lowest flow rate, resulting in approximately 200–500 events per second, and reanalysed with a target value of >95% of positive cells. Samples were collected in a tube containing 50 µl $DM3_{\Phi}$ to avoid cell damage during the collection process. All data analysis was done using FlowJo v10.6.1 (BD Biosciences).

Data analysis and visualization

Data analysis and plotting of data were performed in Graphpad Prism v8.0, except for FACS and MS data.

Reporting summary

Further information on research design is available in the Nature Portfolio Reporting Summary linked to this article.

Data availability

Data can be accessed via the Source Data files and Supplementary Tables provided with this paper. Representative cryotomograms have been deposited in the EMDB database under accession codes EMD-16284–EMD-16291 and EMD-16305–EMD-16306. Source data are provided with this paper.

References

1. Pang, T., Savva, C. G., Fleming, K. G., Struck, D. K. & Young, R. Structure of the lethal phage pinhole. *Proc. Natl Acad. Sci. USA* **106**, 18966–18971 (2009).
2. Wendlinger, G., Loessner, M. J. & Scherer, S. Bacteriophage receptors on *Listeria monocytogenes* cells are the N-acetylglucosamine and rhamnose substituents of teichoic acids or the peptidoglycan itself. *Microbiology* **142**, 985–992 (1996).
3. Dunne, M., Hupfeld, M., Klumpp, J. & Loessner, M. J. Molecular basis of bacterial host interactions by gram-positive targeting bacteriophages. *Viruses* **10**, 397 (2018).
4. Bertozzi Silva, J., Storms, Z. & Sauvageau, D. Host receptors for bacteriophage adsorption. *FEMS Microbiol. Lett.* **363**, 1–11 (2016).
5. Cahill, J. & Young, R. Phage lysis: multiple genes for multiple barriers. *Adv. Virus Res.* **103**, 33–70 (2019).
6. Young, R. Phage lysis: do we have the hole story yet? *Curr. Opin. Microbiol.* **16**, 790–797 (2013).
7. Loessner, M. J. Bacteriophage endolysins - current state of research and applications. *Curr. Opin. Microbiol.* **8**, 480–487 (2005).
8. Schmelcher, M., Donovan, D. M. & Loessner, M. J. Bacteriophage endolysins as novel antimicrobials. *Future Microbiol.* **7**, 1147–1171 (2012).
9. Diaz, E., Lopez, R. & Garcia, J. L. Chimeric phage-bacterial enzymes: a clue to the modular evolution of genes. *Proc. Natl Acad. Sci. USA* **87**, 8125–8129 (1990).
10. Wang, I. N., Smith, D. L. & Young, R. Holins: the protein clocks of bacteriophage infections. *Annu. Rev. Microbiol.* **54**, 799–825 (2000).
11. Toyofuku, M., Nomura, N. & Eberl, L. Types and origins of bacterial membrane vesicles. *Nat. Rev. Microbiol.* **17**, 13–24 (2019).
12. Turnbull, L. et al. Explosive cell lysis as a mechanism for the biogenesis of bacterial membrane vesicles and biofilms. *Nat. Commun.* **7**, 11220 (2016).
13. Toyofuku, M. et al. Prophage-triggered membrane vesicle formation through peptidoglycan damage in *Bacillus subtilis*. *Nat. Commun.* **8**, 481 (2017).
14. Kawai, Y., Mickiewicz, K. & Errington, J. Lysozyme counteracts β-lactam antibiotics by promoting the emergence of L-form bacteria. *Cell* **172**, 1038–1049 (2018).
15. Dell'Era, S. et al. *Listeria monocytogenes* L-forms respond to cell wall deficiency by modifying gene expression and the mode of division. *Mol. Microbiol.* **73**, 306–322 (2009).
16. Errington, J., Mickiewicz, K., Kawai, Y., Wu, L. J. & Errington, J. L-form bacteria, chronic diseases and the origins of life. *Phil. Trans. R. Soc. B* **371**, 20150494 (2016).
17. Mickiewicz, K. M. et al. Possible role of L-form switching in recurrent urinary tract infection. *Nat. Commun.* **10**, 4379 (2019).
18. Domingue, G. J. & Woody, H. B. Bacterial persistence and expression of disease. *Clin. Microbiol. Rev.* **10**, 320–344 (1997).
19. Mercier, R., Domínguez-Cuevas, P., Errington, J., Mercier, R. & Domı, P. Crucial role for membrane fluidity in proliferation of primitive cells. *Cell Rep.* **1**, 417–423 (2012).
20. Taubeneck, U. Der Einfluß von Bakteriophagen auf die L-Phase von *Proteus mirabilis*. *Z. Naturforsch. B* **13B**, 471–472 (1958).
21. Schuhmann, E. & Taubeneck, U. Stabile L-Formen verschiedener *Escherichia coli*-Stämme. *Z. Allg. Mikrobiol.* **9**, 297–313 (1969).
22. Ongenae, V. et al. Reversible bacteriophage resistance by shedding the bacterial cell wall. *Open Biol.* **12**, 210379 (2022).
23. Fabijan, A. P. et al. L-form switching in Escherichia coli as a common β-lactam resistance mechanism. *Microbiol. Spectr.* **10**, e0241922 (2022).
24. Kilcher, S., Studer, P., Muessner, C., Klumpp, J. & Loessner, M. J. Cross-genus rebooting of custom-made, synthetic bacteriophage genomes in L-form bacteria. *Proc. Natl Acad. Sci. USA* **115**, 567–572 (2018).
25. Allan, E. J., Hoischen, C. & Gumpert, J. Bacterial L-forms. *Adv. Appl. Microbiol.* **68**, 1–39 (2009).
26. Leaver, M., Domínguez-Cuevas, P., Coxhead, J. M., Daniel, R. A. & Errington, J. Life without a wall or division machine in *Bacillus subtilis*. *Nature* **457**, 849–853 (2009).
27. Mercier, R., Kawai, Y. & Errington, J. Excess membrane synthesis drives a primitive mode of cell proliferation. *Cell* **152**, 997–1007 (2013).
28. Studer, P. et al. Proliferation of *Listeria monocytogenes* L-form cells by formation of internal and external vesicles. *Nat. Commun.* **7**, 13631 (2016).
29. Klumpp, J. & Loessner, M. J. *Listeria* phages: genomes, evolution, and application. *Bacteriophage* **3**, e26861 (2013).
30. Meile, S. et al. Engineered reporter phages for rapid bioluminescence-based detection and differentiation of viable Listeria cells. *Appl. Environ. Microbiol.* **86**, e00442-20 (2020).
31. Osuna, B. A. et al. *Listeria* phages induce Cas9 degradation to protect lysogenic genomes. *Cell Host Microbe* **28**, 31–40 (2020).
32. Luria, S. E. & Steiner, D. L. The role of calcium in the penetration of bacteriophage T5 into its host. *J. Bacteriol.* **67**, 635–639 (1954).
33. Rountree, P. M. The role of divalent cations in the multiplication of staphylococcal bacteriophages. *J. Gen. Microbiol.* **12**, 275–287 (1955).
34. Rountree, P. M. The role of certain electrolytes in the adsorption of staphylococcal bacteriophages. *J. Gen. Microbiol.* **5**, 673–680 (1951).
35. Mercier, R., Kawai, Y. & Errington, J. General principles for the formation and proliferation of a wall-free (L-form) state in bacteria. *eLife* **3**, e04629 (2014).
36. Briers, Y. et al. Intracellular vesicles as reproduction elements in cell wall-deficient L-form bacteria. *PLoS ONE* **7**, e38514 (2012).
37. Schmelcher, M. et al. Rapid multiplex detection and differentiation of *Listeria* cells by use of fluorescent phage endolysin cell wall binding domains. *Appl. Environ. Microbiol.* **76**, 5745–5756 (2010).
38. Medeiros, J. M., Böck, D. & Pilhofer, M. Imaging bacteria inside their host by cryo-focused ion beam milling and electron cryotomography. *Curr. Opin. Microbiol.* **43**, 62–68 (2018).
39. Loessner, M. J., Kramer, K., Ebel, F. & Scherer, S. C-terminal domains of *Listeria monocytogenes* bacteriophage murein hydrolases determine specific recognition and high-affinity binding to bacterial cell wall carbohydrates. *Mol. Microbiol.* **44**, 335–349 (2002).
40. Sumrall, E. T. et al. Glycotyping and specific separation of *Listeria monocytogenes* with a novel bacteriophage protein tool kit. *Appl. Environ. Microbiol.* **86**, e00612–e00620 (2020).
41. Ujmajuridze, A. et al. Adapted bacteriophages for treating urinary tract infections. *Front. Microbiol.* **9**, 1832 (2018).
42. Meile, S., Du, J., Dunne, M., Kilcher, S. & Loessner, M. J. Engineering therapeutic phages for enhanced antibacterial efficacy. *Curr. Opin. Virol.* **52**, 182–191 (2022).
43. Du, J. et al. Enhancing bacteriophage therapeutics through in situ production and release of heterologous antimicrobial effectors. Preprint at *bioRxiv* https://doi.org/10.1101/2022.03.09.483629 (2022).
44. Labrie, S. J., Samson, J. E. & Moineau, S. Bacteriophage resistance mechanisms. *Nat. Rev. Microbiol.* **8**, 317–327 (2010).
45. Sørensen, M. C. H. et al. *Campylobacter* phages use hypermutable polyG tracts to create phenotypic diversity and evade bacterial resistance. *Cell Rep.* **35**, 109214 (2021).
46. Grosboillot, V., Keller, I., Ernst, C., Loessner, M. J. & Schuppler, M. Ampicillin treatment of intracellular *Listeria monocytogenes* triggers formation of persistent, drug-resistant L-form cells. *Front. Cell Infect. Microbiol.* **12**, 869339 (2022).

47. Chang, S. & Cohen, S. N. High frequency transformation of *Bacillus subtilis* protoplasts by plasmid DNA. *Mol. Gen. Genet.* **168**, 111–115 (1979).
48. Sambrook, J., Fritsch, E. F. & Maniatis, T. In *Molecular Cloning: A Laboratory Manual* 11–14 (Cold Spring Harbor Laboratory, 1989).
49. Monk, I. R., Gahan, C. G. M. & Hill, C. Tools for functional postgenomic analysis of *Listeria monocytogenes*. *Appl. Environ. Microbiol.* **74**, 3921–3934 (2008).
50. Seijsing, J. et al. Improved biodistribution and extended serum half-life of a bacteriophage endolysin by albumin binding domain fusion. *Front. Microbiol.* **9**, 2927 (2018).
51. Schmelcher, M. et al. Evolutionarily distinct bacteriophage endolysins featuring conserved peptidoglycan cleavage sites protect mice from MRSA infection. *J. Antimicrob. Chemother.* **70**, 1453–1465 (2014).
52. Korndörfer, I. P. et al. The crystal structure of the bacteriophage PSA endolysin reveals a unique fold responsible for specific recognition of *Listeria* cell walls. *J. Mol. Biol.* **364**, 678–689 (2006).
53. Iancu, C. V. et al. Electron cryotomography sample preparation using the Vitrobot. *Nat. Protoc.* **1**, 2813–2819 (2007).
54. Tivol, W. F., Briegel, A. & Jensen, G. J. An improved cryogen for plunge freezing. *Microsc. Microanal.* **14**, 375–379 (2008).
55. Mastronarde, D. N. Automated electron microscope tomography using robust prediction of specimen movements. *J. Struct. Biol.* **152**, 36–51 (2005).
56. Mastronarde, D. N. Correction for non-perpendicularity of beam and tilt axis in tomographic reconstructions with the IMOD package. *J. Microsc.* **230**, 212–217 (2008).
57. Kremer, J. R., Mastronarde, D. N. & McIntosh, J. R. Computer visualization of three-dimensional image data using IMOD. *J. Struct. Biol.* **116**, 71–76 (1996).

Acknowledgements

We thank M. Wickert from the Cytometry Facility at UZH Zürich for technical support with FACS; S. Chesnov from the Functional Genomics Center Zürich for mass spectrometry analysis of Ply007; the imaging platform ScopeM for instrument access and P. Studer for advice in the preparation of the grant proposal. This work was supported by the Swiss National Science Foundation (SNSF) Grant 31003A_170042 to M.J.L. Open access funding provided by Swiss Federal Institute of Technology Zurich.

Author contributions

M.S. and M.J.L. planned the project. J.C.W., M.J.L., M.F. and M.S. designed the research. J.C.W., M.F., A.S. and M.B. performed the experiments. S.M. provided the *E. faecalis* Rev strain. J.C.W., A.S., M.F. and M.B. analysed the data. J.W. wrote and revised the manuscript, with input from all authors. S.K. provided important input during manuscript revision. M.J.L., M.S. and M.P. supervised the project.

Competing interests

The authors declare no competing interests.

Additional information

Supplementary information The online version contains supplementary material available at https://doi.org/10.1038/s41564-022-01317-3.

Correspondence and requests for materials should be addressed to Martin J. Loessner.

Peer review information *Nature Microbiology* thanks Romain Mercier, Martha Clokie and the other, anonymous, reviewer(s) for their contribution to the peer review of this work.

Reprints and permissions information is available at www.nature.com/reprints.

Publisher's note Springer Nature remains neutral with regard to jurisdictional claims in published maps and institutional affiliations.

nature portfolio

Corresponding author(s): Martin J. Loessner

Last updated by author(s): Dec 12, 2022

Reporting Summary

Nature Portfolio wishes to improve the reproducibility of the work that we publish. This form provides structure for consistency and transparency in reporting. For further information on Nature Portfolio policies, see our Editorial Policies and the Editorial Policy Checklist.

Statistics

For all statistical analyses, confirm that the following items are present in the figure legend, table legend, main text, or Methods section.

n/a	Confirmed	
☐	☒	The exact sample size (*n*) for each experimental group/condition, given as a discrete number and unit of measurement
☐	☒	A statement on whether measurements were taken from distinct samples or whether the same sample was measured repeatedly
☒	☐	The statistical test(s) used AND whether they are one- or two-sided *Only common tests should be described solely by name; describe more complex techniques in the Methods section.*
☒	☐	A description of all covariates tested
☒	☐	A description of any assumptions or corrections, such as tests of normality and adjustment for multiple comparisons
☐	☒	A full description of the statistical parameters including central tendency (e.g. means) or other basic estimates (e.g. regression coefficient) AND variation (e.g. standard deviation) or associated estimates of uncertainty (e.g. confidence intervals)
☒	☐	For null hypothesis testing, the test statistic (e.g. *F*, *t*, *r*) with confidence intervals, effect sizes, degrees of freedom and *P* value noted *Give P values as exact values whenever suitable.*
☒	☐	For Bayesian analysis, information on the choice of priors and Markov chain Monte Carlo settings
☒	☐	For hierarchical and complex designs, identification of the appropriate level for tests and full reporting of outcomes
☒	☐	Estimates of effect sizes (e.g. Cohen's *d*, Pearson's *r*), indicating how they were calculated

Our web collection on statistics for biologists contains articles on many of the points above.

Software and code

Policy information about availability of computer code

Data collection	cryoET imaging: Tilt series and 2D projection images were acquired using SerialEM 3.7. Data for time course turbidity assays, fluorescence assays, and enzymatic assays were acquired using Omega Software v5.10. Flow cytometry data were collected using Diva 8.01 software (BD Biosciences). Mass spectrometry data were recorded with the MassLynx 4.2 Software (Waters). Microscopic images were acquired using Leica application suite software v. 2.5.1.6757.
Data analysis	Tomogram reconstruction: Drift-correction and exposure-filtering was conducted using Alignframes. Three-dimensional reconstructions and segmentations were calculated using IMOD software package. Flow cytometry: Data analysis was done using FlowJo v10.6.1 (BD Biosciences). Time course turbidity, fluorescence and enzymatic assays: Data analysis and plotting of data was performed in Prism v.8.0 (Graphpad Software). Mass spectrometry: The recorded m/z data were individually deconvoluted into mass spectra by applying the maximum entropy algorithm MaxEnt1 (MaxLynx). Microscopy: Image analysis and processing was performed using Fiji v.1.51.

For manuscripts utilizing custom algorithms or software that are central to the research but not yet described in published literature, software must be made available to editors and reviewers. We strongly encourage code deposition in a community repository (e.g. GitHub). See the Nature Portfolio guidelines for submitting code & software for further information.

Data

Policy information about availability of data

All manuscripts must include a data availability statement. This statement should provide the following information, where applicable:

- Accession codes, unique identifiers, or web links for publicly available datasets
- A description of any restrictions on data availability
- For clinical datasets or third party data, please ensure that the statement adheres to our policy

Representative cryo-tomograms have been deposited in the EMDB database () under accession codes: EMD-16284 – EMD-16291 and EMD-16305 – EMD-16306. Data can be accessed via the Source Data files and Supplementary Tables provided with this paper.

Human research participants

Policy information about studies involving human research participants and Sex and Gender in Research.

Reporting on sex and gender	N/A
Population characteristics	N/A
Recruitment	N/A
Ethics oversight	N/A

Note that full information on the approval of the study protocol must also be provided in the manuscript.

Field-specific reporting

Please select the one below that is the best fit for your research. If you are not sure, read the appropriate sections before making your selection.

☒ Life sciences ☐ Behavioural & social sciences ☐ Ecological, evolutionary & environmental sciences

For a reference copy of the document with all sections, see nature.com/documents/nr-reporting-summary-flat.pdf

Life sciences study design

All studies must disclose on these points even when the disclosure is negative.

Sample size	N/A
Data exclusions	No data were excluded.
Replication	All experiments were conducted at least in biological triplicates.
Randomization	No experimental groups were allocated in this study.
Blinding	Blinding is not applicable for this study.

Reporting for specific materials, systems and methods

We require information from authors about some types of materials, experimental systems and methods used in many studies. Here, indicate whether each material, system or method listed is relevant to your study. If you are not sure if a list item applies to your research, read the appropriate section before selecting a response.

Materials & experimental systems

n/a	Involved in the study
☒	☐ Antibodies
☒	☐ Eukaryotic cell lines
☒	☐ Palaeontology and archaeology
☒	☐ Animals and other organisms
☒	☐ Clinical data
☒	☐ Dual use research of concern

Methods

n/a	Involved in the study
☒	☐ ChIP-seq
☐	☒ Flow cytometry
☒	☐ MRI-based neuroimaging

Flow Cytometry

Plots

Confirm that:

☒ The axis labels state the marker and fluorochrome used (e.g. CD4-FITC).

☒ The axis scales are clearly visible. Include numbers along axes only for bottom left plot of group (a 'group' is an analysis of identical markers).

☒ All plots are contour plots with outliers or pseudocolor plots.

☒ A numerical value for number of cells or percentage (with statistics) is provided.

Methodology

Sample preparation	For analysis of phage-induced eGFP fluorescence, mid-exponential L. monocytogenes strain Rev2 cells expressing RFP cells were diluted to an OD(600 nm) of 0.1. 190 µl of the diluted sample were infected with 10 µl A006::egfpcps 108 PFU at 30°C. Samples were incubated for 45, 60, 75 or 120 min and diluted 1:50 in flow cytometry grade PBS, pH7.4. Diluted samples were immediately analysed from a 1.5 ml tube with no swirling at 4°C.
Instrument	BD FACS Aria III cell sorting device
Software	FlowJo v10.0.6
Cell population abundance	No cell population sorting was conducted.
Gating strategy	Prior to experiments, voltage settings for the relevant fluorescence channels were adjusted by running L. monocytogenes strain Rev2 walled cells expressing no fluorescent proteins or eGFP or RFP. Forward scatter (FSC-H) and side scatter (SSC-H) threshold values were set to 500 to minimize noise. For all experiments, bacterial cells expressing chromosomally integrated RFP were used. Bacterial events were identified based on scatter (FSC-H)- and RFP fluorescence intensity. To eliminate doublets, serial dilutions of bacteria were run to determine the linear range of the event rate

☒ Tick this box to confirm that a figure exemplifying the gating strategy is provided in the Supplementary Information.